



Contents lists available at ScienceDirect

Scripta Materialia

journal homepage: www.elsevier.com/locate/scriptamat

Understanding mechanical behavior of metallic foam with hollow struts using the hollow pentagonal dodecahedron model

Rui Dai^a, Meng Wang^c, Dini Wang^b, Zengrong Hu^d, Matthew D. Green^c, Qiong Nian^{a,b,*}

^a Department of Mechanical Engineering, United States

^b Department of Material Science and Engineering, School of Engineering for Matter, Transport and Energy, Arizona State University, Tempe, AZ 85281, United States

^c Department of Chemical Engineering, School of Engineering for Matter, Transport and Energy, Arizona State University, Tempe, AZ 85281, United States

^d School of Rail Transportation, Soochow University, Suzhou, Jiangsu, 215131, China

ARTICLE INFO

Article history:

Received 8 January 2020

Revised 1 March 2020

Accepted 2 March 2020

Available online xxx

Keywords:

Cellular material

Metallic foam

Hollow strut

Pentagonal dodecahedron

Elastic modulus

ABSTRACT

Nickel (Ni) foam with hollow struts, as one type of ultralight stochastic cellular material, can be simply manufactured by electroplating on a thermally or chemically removable template. A fundamental understanding is required to create a consistent lattice model with capability to capture its mechanical behavior. Herein, an unprecedented hollow pentagonal dodecahedron (HPD) model is proposed with a novel 3D packing architecture. HPD model reveals the scaling of Young's modulus (E) to relative density (ρ') in the factor of 2, which agrees well with uniaxial compression tests. This simplified model paves a way to investigate the cellular material with hollow struts.

© 2020 Acta Materialia Inc. Published by Elsevier Ltd. All rights reserved.

Mechanical metamaterials, either periodically or stochastically architected from nanoscale to microscale, are able to combine structure and host material together and thus enable a wide range of material properties not commonly found in nature [1]. Cellular metallic material is one such subset, which attracts enormous attention in applications ranging from structure supporting frames to passive heat dissipation, battery electrodes, automotive, railway, and etc. [2]. The increased interests in cellular metallic materials is attribute to their exceptional characteristics including high strength-to-weight ratio, light weight, super large surface area combining with excellent thermal and electrical properties [3].

These cellular metallic materials can be manufactured through precision casting [4], powder metallurgy [5], injection molding [6,7], polymer templated deposition [8], or additive manufacturing [9], and can either be closed or open cell, stochastic, or periodic in architecture [10]. It is noteworthy that in recent years the versatility of manufacturing for various metal alloys (Ni-P, Ni-Cu, Ni-W-P) [11] with electroless-electroplating and additive manufacturing for polymer templates [12] engenders unbound potential design space by which new cellular metallic material can be created, including both stochastic and topology-optimized architectures. For

instance, Queheillalt et al. [13] manufactured stochastic open cell metal foam through polymer templated physical vapor deposition. The deposition process is based on an open-cell polymer foam template, e.g., polyurethane (PU) foam, upon which a conformal metal alloy layer is deposited onto the surface of the struts. Using a similar strategy, but with cost-effective electroless-electroplating method, Schaedler et al. [11] created a novel periodical Nickel (Ni) based micro-lattice with structural hierarchy spanning from nanometers to millimeters. The author showed that the architected structure can achieve efficient material utilization, with the Young's modulus scaling as $E \sim \rho'^2$, and was able to recover from more than 50% compression deformation at ultralight densities (relative densities of $< 0.1\%$), which demonstrates large kinetic energy absorption ability upon cyclic loading. Additionally, this electroless-electroplating method has been utilized to manufacture stochastic Ni foam by Jung et al. [14], during which the authors concluded that the polymer template core only had a marginal effect on the mechanical properties and hence can be neglected for performance analysis.

Despite a number of studies have been conducted, there are still challenges related to the structural interpretation of those cellular metallic materials, especially with hollow struts. For example, few studies delve into the stochastic architecture enhancement of metal alloy structure on the polymer template, how the metal alloy enhancement occurs, and to what extend the enhancement

* Corresponding author.

E-mail address: qiong.nian@asu.edu (Q. Nian).

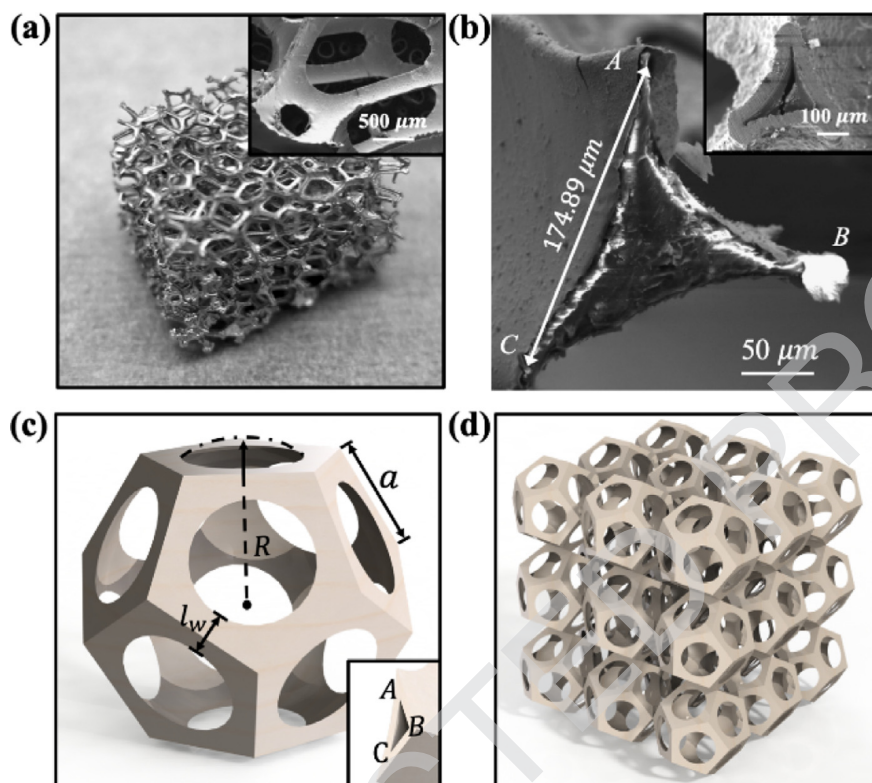


Fig. 1. (a) Optical image of the open-cell Ni foam, insert is the architecture of the copper coated PU foam as the template. (b) Representative SEM image of a single strut in copper coated PU foam template, insert is the hollow Ni strut after template removal. (c) A unit cell of HPD model and its lattice parameters. (d) 3D packing of the HPD unit cells.

could be. And, few guiding principles exist for designing the foam-like architecture that efficiently integrates the structure and microstructural deformation mechanisms [4,10]. Most previous studies concentrate on the modeling of cellular metallic materials, but with solid struts, such as Kelvin structures [15] and Weaire-Phelan structures [16], both of which were developed on the idea of the surface area minimization. Kwon et al. [17], developed a Tetrakaidecahedral frame structure as a representative unit-cell that can predict the stiffness of metallic foam agreeing well with experimental data. X-ray computed tomography is also used for cellular solids modeling, though prior studies reported that the prediction leads to a systematic overestimation of the elastic properties [18]. To the authors' knowledge, an architected model that can describe the elastic behavior of cellular metallic material with hollow struts remains rare. In addition, unlike topology optimized structures, stochastic structures bring extra challenges due to not only the uncertainty combination of their underline lattice but also the reticulation and the redundancy of these combinations. Nevertheless, understanding the complex interplay between the topology of the hollow strut foam structure and the constituent materials is crucial for optimizing and designing complex topological structures with tunable mechanical properties.

In this work, an unprecedented hollow pentagonal dodecahedron (HPD) lattice model is developed to study the mechanical behavior of the stochastic metallic foam with hollow struts, which is manufactured by PU foam templating and Ni electroless-electroplating as shown in Fig. 1(a). This templated Ni foam normally possesses a uniform three-dimensional reticulated structure that is comprised of various unit cells with different size and shape suggesting an isotropic architecture. Fig. 1(b) shows the geometrical size and shape of a single strut (insert shows the hollow Ni strut, more details seen in supporting materials). To mimic the

architecture of this as-manufactured stochastic foam, a pentagonal dodecahedron (PD) model following prior studies [19–21] has been developed, but with an innovative strategy to create hollow struts for the first time (more details seen in supporting materials) in Fig. 1(c). This HPD unit cell is chosen as a representative volume elementary (RVE), while a novel 3D packing architecture for HPD lattices is proposed to enable a potential periodic boundary condition (PBC) as shown in Fig 1(d). Then, Finite Element Method (FEM) simulations are applied on the as-built monolithic unit cell with Ni as the constituent material to assess its capability of interpreting the mechanical behavior of Ni foam with hollow struts. The simulation results are validated by comparing to both the experimental compression tests and the theoretical power coefficient law drawn from an analytical model considering the bending, stretching and shearing behavior of representative strut as Timoshenko beam subject to the uniaxial compression stress. Moreover, the stress distribution on struts are studied to understand the potential mechanical failure (fracture) of the HPD lattice architecture.

Fig. 2 shows the compression behavior of an HPD unit cell in the wall thickness of 25 μm. Stress contours of 0.2%, 1%, 2% and 3% volume averaged strain are shown in Fig. 2(a) – (d). At a small strain of 0.2%, it is clear to observe the stress concentration in the HPD lattice starts to appear near the end of the struts, implying the collapse of the struts always tend to occur near the clamped area. This is corresponding to the theory that plastic deformation always originates near or at the “node” region [22]. As the deformation continues to larger strain, plastic deformation will propagate through the whole struts indicating the whole structure reaches the plastic deformation stage and the struts may start to collapse by the plastic localization (i.e. buckling and necking). [23,24] Besides, the uneven stress distribution across different struts implies they will not fail at the same time leading to the consecutive

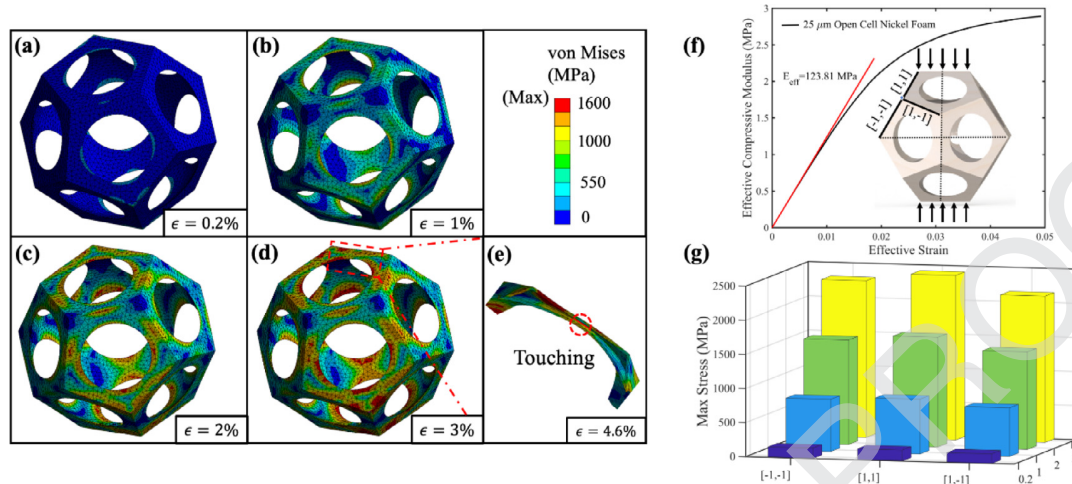


Fig. 2. (a)-(d) The stress contour of the HPD unit cell deformed under a series of volume averaged strains; (e) a cross-section view of the inner surface of a hollow strut deformed under 5.3% volume averaged strain; (f) engineering stress-strain curve of the HPD unit cell with wall thickness of 25 μm , note: the modulus is derived from the first 0.2% effective strain assumed to be linear. The inset image shows the struts of the HPD unit are classified to three different types; (g) Statistical analysis showing the maximum equivalent stress on the outer surface around the center of the three different types of struts.

111 failure of the lattice structure. This phenomenon has been demon-
 112 strated by prior experiments as well. For example, Torrent et al.
 113 [10] showed that the failures on the strut structure were a main
 114 reason leading to the decrease of the mechanical strength of
 115 cellular metallic material. Whereas, for this hollow structure, the
 116 outer surface generally exhibits larger deformation than the inner
 117 surface. As a result, the breaks will occur on the outer surface
 118 first followed by the inner surface; therefore, there won't be a
 119 steep stress drop during compression, which contrasts with solid
 120 counterpart materials. As the deformation continues to around
 121 4.6% volume averaged strain as shown in Fig. 2(e), the inner
 122 surface and the outer surface will be in contact with each other
 123 resulting in a reinforcement on the strength of the beam. These
 124 results demonstrate that a superior mechanical property could be
 125 achieved by applying a hollow strut structure compared to a solid
 126 strut, especially at the same relative density level, which agrees
 127 well with Queheillat's results [13].

128 To interpret which strut initiates the mechanical failure in our
 129 HPD architecture, we classified all the struts into three types with
 130 respect to their position considering the symmetry and ignoring
 131 the PBC boundary struts, as shown in Fig. 2(f). For a quick refer-
 132 ence, these struts are labeled as [1,1], [-1,1] and [1, -1]. The sign
 133 and the number are not the Cartesian coordination while only imply-
 134 ing their rough position. The maximum stress on the surface of
 135 each strut is extracted based on different strain levels shown in
 136 Fig. 2(g). The [-1, -1] strut normally possesses largest stress level
 137 among all strut. From above, it can be concluded [-1, -1] strut is
 138 the start position for the peak stress to reach and the stress on the
 139 plane orthogonal to [-1,1] direction contributes to the formation
 140 of a shear band and eventually a macroscale slip bands evolved.
 141 This phenomenon is also observed by E. Amsterdam [23]. Note this,
 142 for the bending dominated HPD lattice, bending rigidity generated
 143 with the compression of the inner surface and tension of the outer
 144 one, makes it feasible to only consider the stress distribution on
 145 the outer surface of the struts.

146 In order to derive the effective modulus of the Ni foam with
 147 hollow struts, the stress-strain relationship of the HPD lattice ar-
 148 chitecture in the wall thickness of 25 μm is plotted in Fig. 2(f).
 149 Typically, for a cellular metallic structure with the elastic deforma-
 150 tion strain less than 0.2%, the plot tends to be in linear shape. The
 151 slope of the linear curve could be extracted to reflect the effective
 152 modulus of the material. Applying this strategy, the slope of the

153 linear curve in Fig. 2(f) is extracted to be 123 MPa, which is com-
 154 parable to the normalized result of Torrent's study [10]. Note that
 155 the deviation of the modulus results of HPD with prior studies of
 156 Ni micro-lattice is owing to the topology difference between them.
 157 For example, the octet-truss lattice architecture in Torrent's study
 158 has node connectivity of 12, however, the node connectivity is 6
 159 for the 3D packing HPD lattice architecture, suggesting a weaker
 160 mechanical response.

161 The z direction compressive stress-strain response for five rep-
 162 resented HPD unit cells we considered with wall thickness from
 163 10 μm to 50 μm is shown in Fig. 3. The maximum stress value on
 164 the struts, at elastic average volume strain of 0.2%, apparently rises
 165 along with increasing wall thickness in Fig. 3(a). More prominent
 166 stress concentration occurring on the HPD unit with larger wall
 167 thickness can be ascribe to lower strut aspect ratio and larger
 168 material (Ni) mass loading, which induce more significant node
 169 clamping effect. When the wall thickness increases, the mechani-
 170 cal enhancement of the compressive modulus and strength on the
 171 HPD lattice architecture, also can be observed in Fig. 3(b) which is
 172 the stress - strain plots for five different PD units. It is found that
 173 the rate of mechanical enhancement exceeds the rate of Ni materi-
 174 al mass increase as shown in Table 1 with wall thickening. This
 175 can be explained in two folds. One reason can still be ascribed
 176 to the fact mentioned above, that the lower strut aspect ratio
 177 inducing more significant node clamping effect. Another reason is
 178 attribute to the bending dominated deformation behavior of the
 179 hollow strut. In details, for a given strain ϵ , a well-defined stiffness
 180 is around Et , t is the wall thickness, E is Young's modulus of the
 181 constitute material, the tension rigidity and bending rigidity of the
 182 hollow strut can be derived as $Et/(1 - \nu^2)$ and $Et^3/[12(1 - \nu^2)]$,
 183 respectively, where ν is the Poisson ratio. This qualitatively ex-
 184 plains why the compressive modulus of PD lattice architecture
 185 increases much faster comparing to the wall thickness increment.

186 HPD unit cells with wall thickness from 10 μm to 50 μm as
 187 listed in Table 1 are simulated to derive the relationship between
 188 the compressive modulus and relative density of the metallic foam.
 189 Note that the FEM simulations for PD unit cell with wall thickness
 190 less than 10 μm have not been conducted here. This is due to the
 191 extreme thin strut wall in combination with the macroscopic size
 192 of the PD structure, which will induce large computation error.
 193 In addition, usually with such thin strut wall, the roughness and de-
 194 fects will inevitably reduce the foam mechanical strength, and also

Table 1

Summary of geometry properties of HPD lattices.

Thickness (μm)	Volume (10^{-9} m^3)	PD Model Edge Length (mm)	Unit Cell Side Length, L (mm)	Compressive Modulus, E (MPa)	Relative Density, ρ/ρ_s
10	0.196056	1.149520	3.00948278	21.3572	0.007192909
15	0.310754	1.154010	3.02123849	49.9231	0.011268386
20	0.436357	1.158501	3.03299419	80.8553	0.015639657
25	0.572835	1.162991	3.0447499	123.8139	0.020294328
30	0.710157	1.167481	3.0565056	176.2733	0.024870172
35	0.868253	1.171972	3.06826131	244.1481	0.030058635
40	1.037143	1.176462	3.08001701	327.5959	0.035495990
45	1.216795	1.180952	3.09177272	424.7712	0.041171315
50	1.407177	1.185442	3.10352842	542.0802	0.047074048

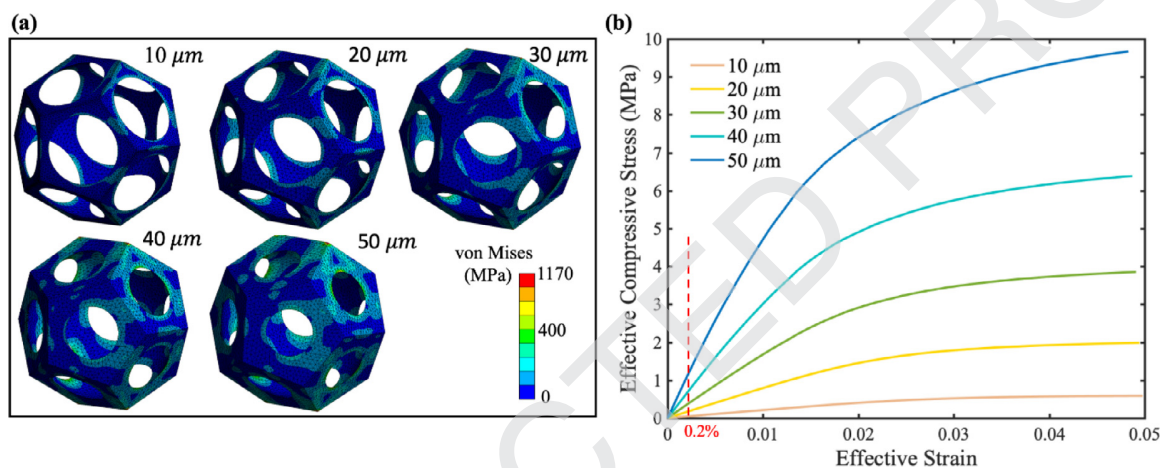


Fig. 3. (a) Schematic diagram of the deformation and stress distribution in HPD unit cell with wall thickness ranging from 10 μm to 50 μm , showing the strain localization (stress concentration) and local buckling of the PD truss; (Note: the stress distribution is rendered at 0.2% effective strain.) (b) The stress-strain curves of HPD model with Ni as the constituent material. (For interpretation of the references to color in this figure legend, the reader is referred to the web version of this article.)

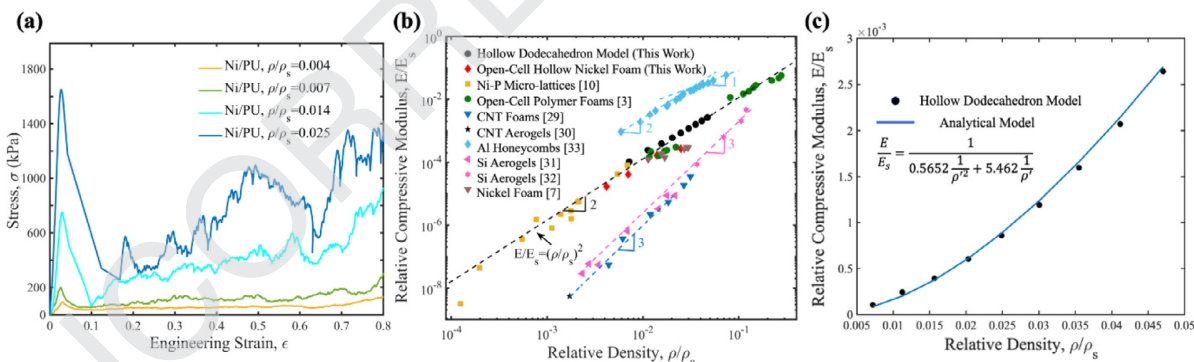


Fig. 4. Modulus and relative density relation: (a) Stress-Strain curves of manufactured Ni foams as a function of the coating thickness; (b) Relative compressive modulus (defined as the measured Young's modulus, E, divided by the Young's modulus of the constituent solid, E_s) of selected cellular materials at low relative density comparing to HPD model results; (c) Quadratic regression fitting for the HPD Model. (For interpretation of the references to color in this figure legend, the reader is referred to the web version of this article.)

195 lead to a prominent difference for the simulation and experiment
196 results [10].

197 To validate the as-developed 3D packing HPD lattice architec-
198 ture for describing mechanical behavior of stochastic metallic foam
199 with hollow struts, the simulation results of effective compressive
200 modulus in Table 1 have been plotted as a function of foam densi-
201 ties and compared to experimental measurements (from both prior
202 studies and this work) in Fig. 4. Fig. 4(a) shows the stress – strain
203 curves of the Ni foam with hollow struts which are manufactured
204 through PU foam templating and electroless-electroplating. The
205 elastic modulus is the maximum slope value obtained by fitting
206 the linear response at small strains found at up to 2.35%, during
207 which the compression and bending of the struts are assumed to

208 dominate the mechanical deformation. The drop of the compressive
209 strength thereafter results from the continuous buckling and
210 failure of struts. [23–26] As observed, both the compressive mod-
211 ulus and strength of the HPD lattice are increasing along with larger
212 wall thickness, which agrees well with the result in Fig. 3. On
213 contrary to thin wall architecture, a distinct stress drops appears
214 in the nickel foam with larger density corresponding to higher wall
215 thickness in Fig. 4(a). To interpret this with our HPD lattice model,
216 as shown in Fig. S1, the maximum stress of the $[-1, -1]$ struts with
217 different wall thickness ranging from 10 to 50 μm are presented.
218 Apparently, the struts with thicker wall bears larger strain local-
219 ization under same effective engineering strain, which is typically
220 attributed to the surface tension of neighbor circle and a shorter

221 effective beam length (due to larger nodal volume) resisting the
 222 deformation [24]. Moreover, the nanocrystalline (NC) nature of
 223 electro-chemical deposited bulk nickel indicates a strong mechan-
 224 ical strength, following the Hall–Petch relation. As small grain size
 225 help reducing the strain accumulation. However, under large deforma-
 226 tion, dislocations can pile up at the grain boundary eventually
 227 resulting a brittle behavior of the NC structure [27,28]. The mod-
 228 ulus of the as-manufactured Ni foam is extracted and compared
 229 with the simulation results in Fig. 4(b). In contrast, other materials
 230 with relative density $< 10 \text{ mg/cm}^3$ are plotted, such as CNT foams
 231 [29,30], silicon aerogel [31,32] and aluminum honeycombs [33]. As
 232 shown, the obtained compressive modulus from the HPD models
 233 with wall thickness ranging from $10 \mu\text{m}$ to $50 \mu\text{m}$, performs a non-
 234 linear mechanical property scaling in the factor of two, which is in
 235 great agreement with the experimental results. Within the low rela-
 236 tive density region ($\rho/\rho_s < 0.01$), a small transition tendency to a
 237 different, topology-dependent scaling relation is observed, result-
 238 ing in an overestimation of the compressive modulus of relative
 239 foam. This deviation is ascribed to the neglected defects in HPD
 240 model, which exist in the actual metallic foam, such as waviness in
 241 the struts [34], non-uniformity of the cross sections [35], misalign-
 242 ment of the nodes, possible defects induced during electroplating
 243 procedure, such as small notches, impurities, oxide layer on the
 244 strut outer surface and precipitates in the cell wall [23,25,26].

245 For the HPD lattice architecture, a transition of the foam stiff-
 246 ness scaling from two to one when the struts decrease slenderness
 247 of $\lambda \approx 20$ ($\rho/\rho_s \approx 0.1$) to $\lambda \approx 1$ ($\rho/\rho_s \approx 0.01$) is identified, where
 248 the slenderness is defined as $\lambda = \sqrt{AL^2/I}$, with A is the cross-
 249 section area, and I is the area moment of inertia of the beam.
 250 Ignoring the combination effects of bending and stretching in
 251 the beam, mechanical properties of lattice architecture normally
 252 modeled with either bending or stretching behavior by assuming
 253 one dominate the other. To understand this transition and address
 254 the complex entanglement of stretching-bending effects as well
 255 as the shear deformation, we developed an analytical model
 256 based on both Euler and Timoshenko beam theory for accurately
 257 capturing the young's modulus of the non-rigid HPD lattice in Fig.
 258 S2. Fitting our model with FEM simulation result, the effective
 259 young's modulus can be expressed with

$$\frac{E}{E_s} = \frac{1}{0.5652 \frac{1}{\rho^{1/2}} + 5.462 \frac{1}{\rho'}} \quad (1)$$

260 Full derivation of this equation is provided in the supple-
 261 ment material. The stiffness transition is similar to the Gibson
 262 and Ashby's (GA) bending dominant model [36], which only has
 263 a squared term in the fit for modulus of elasticity. Moreover, in a
 264 very recent paper, Tereza et al. [37] also numerically calculated the
 265 young's modulus of the GA open cell based metamaterial model
 266 and claims essentially, for the young's modulus, the perfect three
 267 dimensional strut-based metamaterials constructed on open GA
 268 cell don't obey the Gibson-Ashby power law prediction, especially
 269 in the low relative density region. Beside of that, comparing to ex-
 270 perimental results, there are several reasons may affect the stress
 271 and strain behavior of the HPD model at low relative density re-
 272 gion: (1) in HPD model, the struts are defect free and pristine
 273 and thereby bring about the overestimation of the modulus,; (2)
 274 as the thickness increases the node becomes larger and stronger,
 275 which increases the convergence of strength and stiffness in the
 276 lattice at higher density region. Therefore, both simulation artifacts
 277 as well as real structure contribute to the overestimation of the
 278 HPD model for describing the stiffness of the cellular metallic foam
 279 structure in the low density region.

280 In summary, a new approach to modeling and investigating the
 281 mechanical response of hollow Ni foam with periodic 3D packing
 282 HPD lattice architecture is proposed. The elastic response results

283 from the numerical simulations on the uniaxial compression of
 284 the foam were compared to experiments with good agreement. An
 285 in-depth exploration of the mechanical properties using analytical
 286 model assuming Timoshenko beam are provided. Our model not
 287 only provides an insight explanation of the parameter space of
 288 hollow struts-cellular architecture, but also establishes mechanism
 289 of the strength and the stiffness governed by the intricate entan-
 290 glement of geometry and structure. Moreover, it provides a simple
 291 way to accurately predict the mechanical properties of open-cell
 292 cellular foam structure. During our discussion, we postulate that
 293 the convergence of strength and stiffness in the lattice at high
 294 density is caused by the increased influence of the beam intersec-
 295 tions at the node. As the thickness increasing, the node becomes
 296 larger and stronger. However, the strength and stiffness parameter
 297 space of hollow lattices is highly complex and depends not only
 298 on the beam length, radius and thickness but also on the space
 299 topology organization for the full-scale foam. Overall, this work
 300 provides a new prospect to estimate the mechanical properties of
 301 the stochastic cellular structure.

Declaration of Competing Interest

302 The authors declare that they have no known competing finan-
 303 cial interests or personal relationships that could have appeared to
 304 influence the work reported in this paper.
 305

Acknowledgment

306 This study is partially supported by ASU startup funds, NSF
 307 grants CMMI-1825576 and CMMI-1826439. We acknowledge the
 308 use of facilities within the Eyring Materials Center at Arizona State
 309 University supported in part by NNCI-ECCS-1542160. The Instron
 310 E3000 was obtained using funds from the Army Research Office
 311 (W911NF-15-1-0353).
 312

Supplementary materials

313 Supplementary material associated with this article can be
 314 found, in the online version, at doi:10.1016/j.scriptamat.2020.03.
 315 001.
 316

References

- 317
- [1] J. Paulose, A.S. Meussen, V. Vitelli, Proc. Natl. Acad. Sci. 112 (25) (2015) 7639–7644. 318
 - [2] J. Banhart, Prog. Mater. Sci. 46 (6) (2001) 559–632. 319
 - [3] Q. Wang, J.A. Jackson, Q. Ge, J.B. Hopkins, C.M. Spadaccini, N.X. Fang, Phys. Rev. Lett. 117 (17) (2016) 175901. 320
 - [4] I.J. Gibson, M.F. Ashby, Proc. R. Soc. Lond. A 382 (1782) (1982) 43–59. 321
 - [5] G.J. Davies, S. Zhen, J. Mater. Sci. 18 (7) (1983) 1899–1911. 322
 - [6] H.N.G. Wadley, Adv. Eng. Mater. 4 (10) (2002) 726–733. 323
 - [7] M.M. Shbeh, R. Goodall, Met. Powder Rep. 71 (6) (2016) 450–455. 324
 - [8] D.T. Queheillalt, D.D. Hass, D.J. Sypeck, H.N.G. Wadley, J. Mater. Res. 16 (4) (2001) 1028–1036. 325
 - [9] M.G. Rashed, M. Ashraf, R.A.W. Mines, P.J. Hazell, Mater. Des 95 (2016) 518–533. 326
 - [10] A. Torrents, T.A. Schaedler, A.J. Jacobsen, W.B. Carter, L. Valdevit, Acta Mater. 60 (8) (2012) 3511–3523. 327
 - [11] T.A. Schaedler, A.J. Jacobsen, A. Torrents, A.E. Sorensen, J. Lian, J.R. Greer, L. Valdevit, W.B. Carter, Science 334 (6058) (2011) 962–965. 328
 - [12] J.H. Martin, D.S. Ashby, T.A. Schaedler, Mater. Des. 120 (2017) 291–297. 329
 - [13] D.T. Queheillalt, Y. Katsumura, H.N.G. Wadley, Scr. Mater. 50 (3) (2004) 313–317. 330
 - [14] A. Jung, S. Diebels, Adv. Eng. Mater. 18 (4) (2016) 532–541. 331
 - [15] W.E. Warren, A.M. Kraynik, J. Appl. Mech. 64 (4) (1997) 787–794. 332
 - [16] K. Boomsma, D. Poulikakos, Y. Ventikos, Int. J. Heat Fluid Flow 24 (6) (2003) 825–834. 333
 - [17] Y.W. Kwon, R.E. Cooke, C. Park, Mater. Sci. Eng. A 343 (1–2) (2003) 63–70. 334
 - [18] C. Petit, S. Meille, E. Maire, J. Mater. Res. 28 (17) (2013) 2191–2201. 335
 - [19] D.L. Duan, R.L. Zhang, X.J. Ding, S. Li, Mater. Sci. Technol. 22 (11) (2006) 1364–1367. 336
 - [20] T. Fiedler, E. Solórzano, F. Garcia-Moreno, A. Öchsner, I.V. Belova, G.E. Murch, Adv. Eng. Mater. 11 (10) (2009) 843–847. 337

- 348 [21] A. Zenner, D. Edouard, Appl. Therm. Eng. 113 (2017) 1313–1318. 363
349 [22] X.W. Gu, J.R. Greer, Extreme Mech. Lett. 2 (2015) 7–14. 364
350 [23] E. Amsterdam, P.R. Onck, J.T.M. De Hosson, J. Mater. Sci. 40 (22) (2005) 5813– 365
351 5819 0022-2461. 366
352 [24] E. Amsterdam, J.H.B. De Vries, J.T.M. De Hosson, P.R. Onck, Acta Mater. 56 (3) 367
353 (2008) 609–618 1359-6454. 368
354 [25] P.R. Onck, R. Van Merkerk, A. Raaijmakers, J.T.M. De Hosson, J. Mater. Sci. 40 369
355 (22) (2005) 5821–5828 0022-2461. 370
356 [26] P.R. Onck, R. Van Merkerk, J.T.M. De Hosson, I. Schmidt, Adv. Eng. Mater. 6 (6) 371
357 (2004) 429–431 1438-1656. 372
358 [27] J.B. Jeon, B.-J. Lee, Y.W. Chang, Scr. Mater. 64 (6) (2011) 494–497 1359-6462. 373
359 [28] J. Li, B. Lu, H. Zhou, C. Tian, Y. Xian, G. Hu, R. Xia, Phys. Lett. A 383 (16) (2019) 374
360 1922–1928 0375-9601. 375
361 [29] M.A. Worsley, S.O. Kucheyev, J.H. Satcher Jr, A.V. Hamza, T.F. Baumann, Appl. 376
362 Phys. Lett. 94 (7) (2009) 073115 0003-6951. 377
- [30] J. Zou, J. Liu, A.S. Karakoti, A. Kumar, D. Joung, Q. Li, S.I. Khondaker, S. Seal, 363
L. Zhai, ACS Nano 4 (12) (2010) 7293–7302 1936-0851. 364
[31] M. Moner-Girona, A. Roig, E. Molins, E. Martinez, J. Esteve, Appl. Phys. Lett. 75 365
(5) (1999) 653–655 0003-6951. 366
[32] T.M. Tillotson, L.W. Hrubesh, J. Non-Cryst. Solids 145 (1992) 44–50 0022-3093. 367
[33] H.H. Attributes, the technical document issued by the Hexcel composites com- 368
pany, available on the www.hexcel.com internet site (38 pages) (1999) 3. 369
[34] D. Queheillalt, V. Deshpande, H. Wadley, J. Mech. Mater. Struct. 2 (9) (2007) 370
1657–1675 1559-3959. 371
[35] M.A. Fortes, M.F. Ashby, Acta Mater. 47 (12) (1999) 3469–3473 1359-6454. 372
[36] L.J. Gibson, Proc. R. Soc. Lond. A 382 (1782) (1982) 43–59. 373
[37] T. Uhlířová, W. Pabst, Scr. Mater. 159 (2019) 1–4. 374